공학석사 학위논문

Low Density Sound Absorbing Polyurethane Foam via Cell Openness Manipulation

셀 개폐도 제어를 이용한 저밀도 흡음 폴리우레탄 흡음 연구

2017년 8월

서울대학교 대학원

재료공학부

민 경 서

Low Density Sound Absorbing Polyurethane Foam via Cell Openness Manipulation

셀 개폐도 제어를 이용한 저밀도 흡음 폴리우레탄 흡음 연구

지도 교수 윤 재 륜

이 논문을 공학석사 학위논문으로 제출함
2017 년 6 월

서울대학교 대학원
재료공학부
민 경 서

민경서의 석사 학위논문을 인준함
2017 년 6 월

위 원 장 서 용 석 (인)

부위원장 윤 재 륜 (인)

위 원 유 웅 렬 (인)

Abstract

Low Density Sound Absorbing Polyurethane Foam via Cell Openness Manipulation

Kyung Suh Minn

Department of Material & Science Engineering

The Graduate School

Seoul National University

Noise, vibration, and harshness (NVH) characteristics are one of the important factors which determine the high performance luxury vehicle. As NVH performance increases, customer's sensitivity to noise and the quality and satisfaction on the car interior comfort increases. Thus, the choice of excellent sound absorbing material is necessary. Polyurethane foams (PUFs) are widely used as sound absorbers in interior parts of automobiles as well as in other applications in acoustics. The sound absorbing characteristics of acoustical material such as PUF, mostly in open or semi-open cell structure, are majorly dependent on its microstructural change with a variation of frequency.

Cell structure of the PUF can be affected by the ratio between polyurethane resin premix (polyol, cross-linking agent, blowing agent, catalyst) and isocyanate. Furthermore, sound absorption performance of porous media is well-known to be influenced by density and thickness of the foam depending on each different frequency range. In an attempt to satisfy the fabrication of low density sound absorbing semi-open cell PUF, cell openness manipulation method is applied by adding a chemically reactive cell opening agent, polyethylene glycol 2000 (PEG 2000) into the polyol mixture.

Experimentally, a number of pores in PUF were increased by 0, 3 (15% cell openness), and 6 (22% cell openness) wt% of PEG 2000 assuming that cell openness of the PUFs is dependent on the content of PEG 2000. The cell morphologies of the foams were examined using a scanning electron microscopy (SEM). The sound absorption coefficients of each sample were measured by a two-microphone B&K impedance tube. For the comparison of both the experimental and the numerical simulation results, a multiscale modeling involving poroacoustics parameters based on Johnson-Champoux-Allard (JCA) model was developed. This modeling method was used to obtain the sound absorption coefficient of each periodic unit cell (PUC) with four different cell openness (15, 25, 50, and 100%), which are assumed to be the imitation of real fabricated PUF cell structures in ideal conditions.

Further quantitative acoustical analyses *e.g.* a root mean square (RMS) value, a noise reduction coefficient (NRC), and 1/3 octave band spectrogram of the PUFs were conducted. The equivalent comparison between experimental (3 wt% addition of PEG 2000) and simulation results (15% cell openness of PUC) had the best sound absorption performance of PUF (a density of 40 kg/m^3, 500 μm, and thickness of 2 cm). These two results reveal a new potential replacement for conventional PUF used in cars which density (80 kg/m^3) doubles compared to our fabricated sample and which will surpass not only the sound absorption performance, but even improve fuel efficiency by lowering the weight of PUF in the auto industry.

Keywords: NVH; Polyurethane foam; Sound absorption; Cell openness; PEG 2000; JCA model

Student Number: 2015-22744

Contents

List of Tables

List of Figures

Chapter 1. Introduction

1.1 NVH (Noise, Vibration, and Harshness)

The development of noise, vibration, and harshness (NVH) determines a premium automobile brand name in the modern auto industry. Reduction methods of unpleasant NVH while driving bring high customer satisfaction and driving comfort. Hence, automotive manufacturers have invested a lot in research on the development of acoustical foams. Specifically, they focused on how to efficiently minimize noise coming resulting from tires, wind, exhaust, and engine, which are mostly found in low and medium frequency range (Fig. 1 and Table 1.1). Interior and exterior NVH products such as bulk and cavity filling technique are engineered to provide good sound quality for users. Among several acoustical foams, a polyurethane foam (PUF) is a commonly used sound absorber using RIM (reaction injection molding) process [1-2] with rapid cycling and mass production in the manufacturing sector. Adding more advanced properties, such as low uniform density, cost effective, resistance to abrasion, and the improvement of acoustic performance to PUF, will encourage high performance in automotive industry.

1.2 Fundamentals of Polyurethane Foam

Polyurethane foam (PUF) is a wide ranging and well established polymeric foam which has many applications and revolutionized the quality of life. Advantages of PUF compared to other conventional materials *e.g.* metal and ceramic are versatility, flexibility, lightweight, durability, low cost, and etc. These unique properties can be adjusted to produce products in buildings and construction, furniture and bedding, automobile seats and parts, packaging, textiles, fibers and apparel, adhesives, electronics, and more (Fig. 2 (a)).

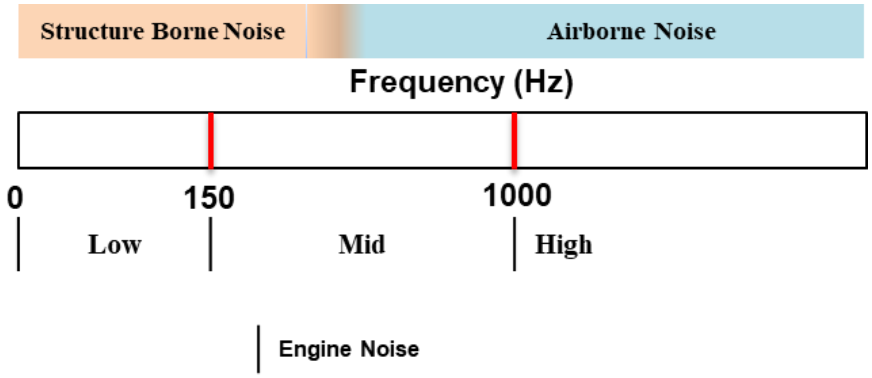

Figure 1. A schematic illustration of structural borne and airbone noise in low, medium, and high frequency range.

Table 1.1
Frequency range of the noise generated by automobile

Sound Source		Frequency (Hz)
Structure Borne Noise (Low + Med)	Airborne Noise (High)	Low : ~ 150 Mid : 150 ~ 1000 High : 1000 ~
<Road Noise> Gear / clutch Noise Booming Noise Wheel Noise	Exhaust Noise Engine Noise	Gear / Clutch Noise (20 – 40) Booming Noise (30 – 100) Wheel Noise (100 – 500) Exhaust Noise (100 – 600) Engine Noise (350 – 10,000)

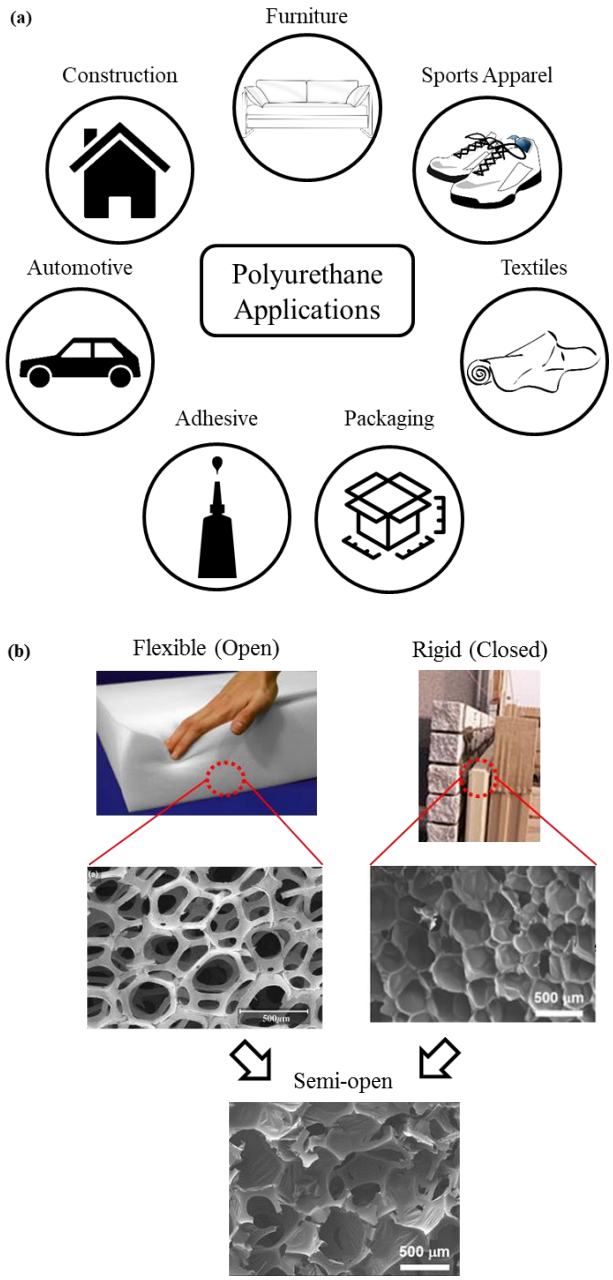

Figure 2. A **s**chematic illustration of (a) polyurethane foam application and (b) the morphology of open [3], closed, and semi-open cell PUF.

Generally, functional properties and applications of PUF can be varied by the morphology of foam (open cell [3], closed cell, semi-open cell), cell size, density, porosity, and etc (Fig. 2 (b)). For example, flexible PUF (open cell, low density, lightly cross-linked) is mostly used for cushioning in furniture, bedding, and footwear. Rigid PUF (closed cell, high density, highly cross-linked) is commonly found in refrigerator walls and building panels for insulation materials. Interestingly however, a combination of flexible and rigid foam, so-called semi-open cell PUF, has been extensively used for an excellent sound absorber in auto-interior parts *e.g.* seats, roof liners, dashboard, and panel. This type of sound absorbing material not only reduces the noise but also protects from shock, impact, and vibration from external force at the same time.

1.3 Sound Absorption in Porous Media

Theories and measurements related to sound absorption and wave propagations of sound in porous media have been proposed over the years [4-7]. A porous material, such as PUF, normally contains a high value of sound absorption coefficient with high porosity (pore volume and pore size distribution of 80 to 90%). In other words, a highly porous material with many pores and channels increases molecular collision rate between air and cell wall or solid frame when sound waves travel through the medium. Figure 3 shows a schematic representation of different pores in a porous material. Pores, which are isolated from the neighbors, are called “closed” pores. However, “open” pores, including “interconnected (throat)” pores or “cross linked” pores, are continuous channels surrounded by solid skeleton or surface boundary which greatly affect the sound absorption. When incident sound waves strike an arbitrary surface, the sound waves or energy are either reflected, transmitted, or absorbed (Fig. 4 (a)). The sound absorption is mainly

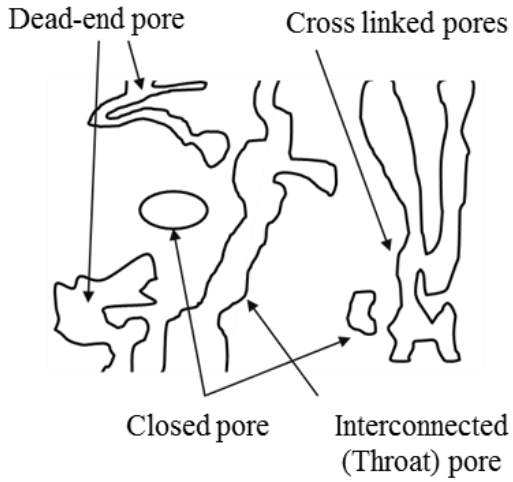

Figure. 3 A schematic representation of pores

caused when a travelling wave enters through the porous medium occurred with two sound damping mechanisms; 'visco-inertial and thermal damping' and 'viscoelastic frame damping' [8-9].

In visco-inertial thermal damping, air molecules from the incident sound waves pass through the porous media by viscous friction on cell walls or struts of the inner cell structure *e.g.* open, closed, and interconnected pores. The contraction and expansion of air pressure convert transferred kinetic energy into thermal energy, called thermal effects, on solid-fluid boundary interface [10-12]. In viscoelastic frame damping, the friction of air molecules in the solid domain dissipates the transferred sound energy to heat loss [5, 13]. It can be said that visco-inertial and thermal damping has a strong influence over the viscoelastic frame damping in total sound absorption behavior. A schematic description of wave propagation in porous media with simultaneous phenomena; viscous friction and thermal exchange, is shown in (Fig. 4 (b)). Thus, a manipulation of cell structure in polymeric foams is expected to be one of the important factors to improve the sound absorption performance.

1.4 Cell Openness Manipulation

The inclusion or reinforcements of *e.g.* short chopped fibres [14], PU/clay nanocomposite [15], PET (polyethylene terephthalate) particle [16], nano- and micro-silica fillers on PUF [17], and CNT (carbon nanotube) [18] in polyurethane foams, were used not only for the enhancement of the sound absorption property but also for the improvements in mechanical, thermal, and other properties. Moreover, noise reduction methods in low and medium frequency range, which most car noises are generated, have been studied [19-20]. These previous outcomes have demonstrated high possibilities of producing new acoustical foam materials, but there were several limitations in industrial applications due to the rupture of foam or defects in the resin. Thus,

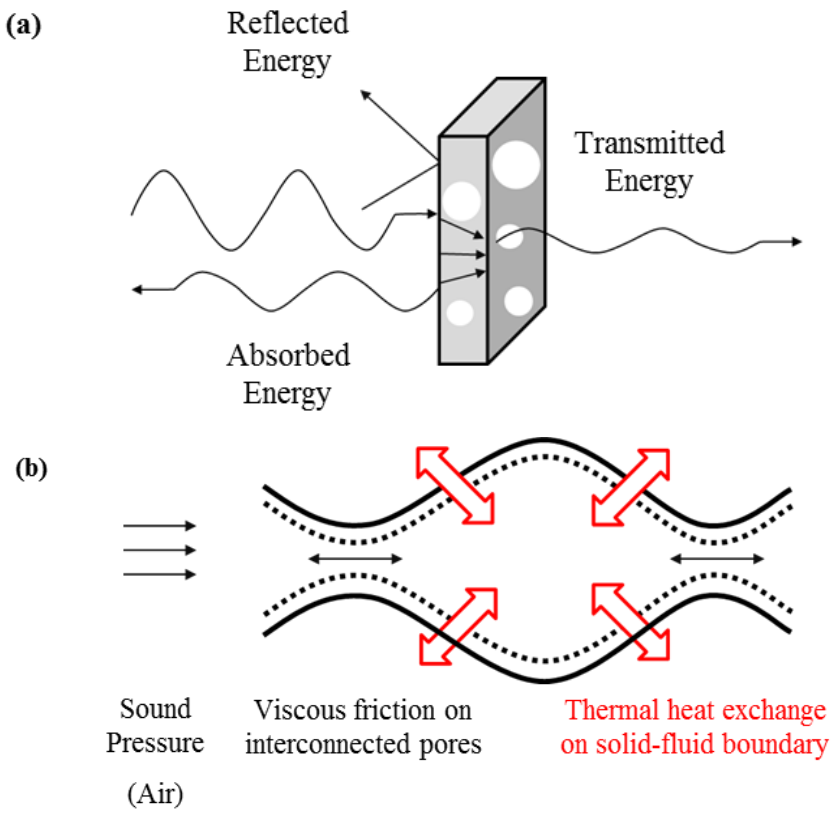

Figure. 4 A schematic description of (a) reflected, transmitted, and absorbed sound energy and (b) wave propagation by viscous friction and thermal exchange in porous media

the control of foam microstructure and other properties is one of the essential treatments to overcome the acoustic damping properties.

As mentioned above, a structural change in porous media plays a crucial role for the enhancement of the sound absorption performance. In previous works, the manipulation of cell size have been controlled using nucleating agents or mechanical excitation in the polymer resin [21-24]. Several studies have attempted to satisfy sound absorption performance with the semi-open cell foam [25-27]. And for the selective cell openings of the foam, a reactive cell opening agent has been introduced by several researchers [28-30]. However in this study, cell openness, another consideration for cell structure, is manipulated with proper opening pores or voids. Cell openness manipulation method is applied to the fabrication of semi-open cell PUF using a chemically reactive cell opening agent. Such semi-open cell PUF is expected to have good sound absorption performance.

1.5 Objective

The purpose of this paper is to investigate the relationship between cell openness (microstructure) manipulation and sound absorption performance of polyurethane foam (PUF). Experimentally, PUFs with the addition of a reactive cell opening agent were fabricated to optimize outstanding sound absorption generating appropriate pores for semi-open cell structure. The microstructural change of PUF was observed through SEM images, and their sound absorption coefficients were measured using a B&K impedance tube. Second, numerical simulation results by evaluating poroacoustics parameters of periodic unit cells (PUC's) were compared with experimental results. The unit cells were constructed to analyze each different cell openness of the foam in ideal case. Then, acoustical parameters were obtained from multiscale modeling method solving microscale flow analyses. And the sound absorption

coefficients imported from the acoustical parameters were computed from the imitation of real B&K impedance tube design, a macroscale geometry. The most influential factor in both experimental and numerical studies was tortuosity, simply the ratio of complexity of flow path. Moreover, the optimal process condition for sound absorbing PUF was confirmed in low and medium frequency range, satisfying both the improvements of noise reduction and the weight reduction of the foam. In addition, this work is the unprecedented experimental study on cell openness manipulation without changing other material properties. Lastly, this low mass density acoustic foam might have a potential to replace the conventional foam, ensuring high fuel efficiency in auto industry.

Chapter 2. Theoretical Background

2.1 Polyurethane Foam Processing

Cell structures of polyurethane foam (PUF) are classified into three categories: open cell, closed cell, and semi-open cell. Each of them requires the choice of different raw materials, surfactant, blowing agent, catalyst and etc. for suitable applications. Although the components of each different cell structure may vary, the manufacturing process and the foaming reaction are occurred in the same way. Specifically, the exothermic reactions between alcohols (-OH groups such as diols, triols and polyols) and isocyanates (-NCO group such as diisocyanates and polyisocyanates) are generated when the two mixture are rapidly mixed in achieving foam expansion.

There exist two simultaneous reactions in the polyurethane resin with the generation of bubbles; blowing reaction and gelling reaction (Fig. 5). A gelling reaction occurs when the –OH groups of polyols meet with –NCO groups of isocyanates and produces a urethane linkage (-$NHCO_2$-). On the other hand, the blowing reaction occurs when the –OH groups of water or other blowing agents react with –NCO groups of isocyanates and produce urea groups (amine group) and carbon dioxide (CO_2) gas. Here, the role of carbon dioxide gas is crucial for the expansion of the foam. Other additives such as surfactants and catalysts are also used for both blowing and gelling reactions for the stabilization of cell structures. By adjusting the appropriate amounts or ratio of basic ingredients (polyol, isocyanate, blowing agent, surfactant, and catalyst) can prevent cell rupture or coalescence which greatly affects the cell opening event of the foam [31].

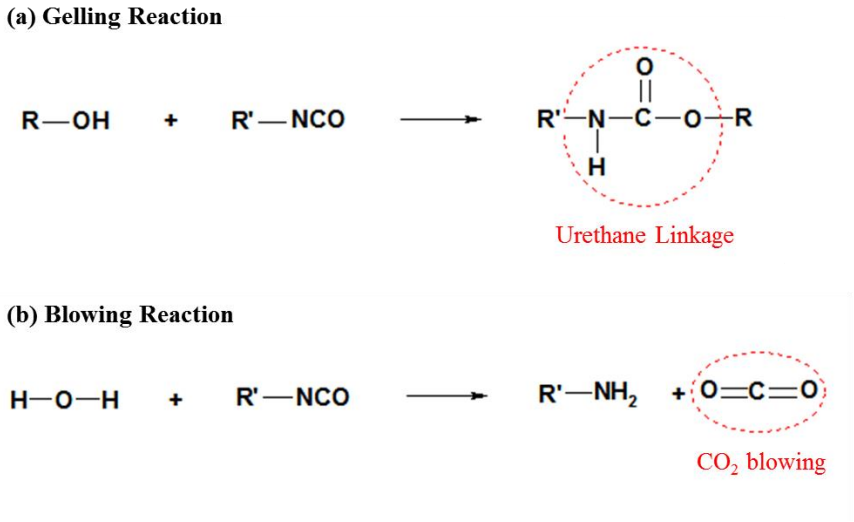

Figure 5. Chemical reaction during PUF formation (a) gelling reaction and (b) blowing reaction.

2.2 Cell Opening Mechanism

Many researchers have worked on the foaming process with various hypotheses on the cell opening mechanism. Saunders and Frisch [32] proposed classical concepts regarding cell opening in flexible foams, the phase separation by adding the surfactant. Frye and Berg [33] proposed the solid particle defoaming from urea precipitation. Neff [34] quantified the internal cell opening time which leads to the extensional thinning and spontaneous rupture of the film. In summary, cell opening mechanism can be characterized by two rheological phenomena; surface rheology control and bulk rheology control. First, surface rheology control is a method of silicone surfactants control which influences the surface tension of the resin [35]. Second, bulk rheology control is dealt with the balance of the gelling and blowing reactions using the catalyst which determine the time of appropriate cell opening [36].

Previous research on the use of reactive cell opening agents were introduced [28-30]. A reactive cell opening agent usually contains high molecular weight including high percentages of –OH group. In this study, poly(ethylene glycol) 2000 (PEG 2000) was selected for a new cell opening agent. When PEG 2000 is reacted with –NCO groups of isocyanate, the balance of gelling and blowing reactions is altered (Fig. 6. (a-b)). The blowing reaction occurs earlier than the gelling reaction and the molecular weight of the polyurethane is decreased. This reduces the viscosity of resin inducing local thinning of the film. Moreover, the thickness of the film is weakened by low elasticity and cannot endure the pressure of CO_2 gas. Then, the rupture of the film or cell wall is eventually occurred. Through this mechanism, the appropriate content of reactive cell opening agent helps in generating open pores for the fabrication of semi-open cell PUF.

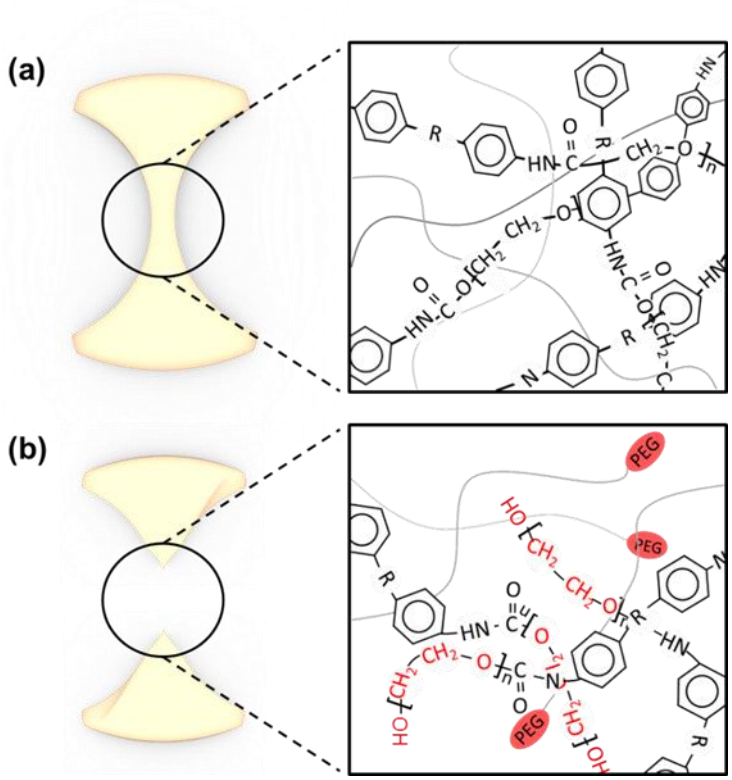

Figure. 6 A schematic representation of a cell opening mechanism between PEG 2000 and –NCO group of isocyanate.

2.3 Modeling of Sound Absorption

A study of sound propagation in straight cylindrical tubes was first developed by the Kirchhoff theory [37]. Yet, the theory was very complicated for many applications in case of non-circular cross section. Zwikker and Kosten [38] elaborated on a simplified model of both visco-inertial and thermal effects between air and the solid in narrow frequency range with circular cross-sections of pores (10^{-3}cm). They claimed that the wave equation (Eqs. 1) for the acoustic pressure inside a tube is:

$$\nabla^2 p + \omega^2 \frac{\rho(\omega)}{K(\omega)} p = 0 \tag{1}$$

where ∇^2 is the Laplacian, ω is the angular frequency, p is the amplitude of acoustic pressure inside the tube, $\rho(\omega)$ is the effective density, and $K(\omega)$ is the bulk modulus of the medium. Both $\rho(\omega)$ and $K(\omega)$ express a complex function of the frequency and the pore shape in porous media. Later, Delany and Bazley [39] in 1970 provided an empirical model with a concept of the characteristic impedance and the complex wave number for porous materials. And, Biot [5, 13, 40] completed the theoretical expression of waves and developed a theory of the motion of the fluid-saturated in pores and the motionless skeleton, rigid frame in porous material both in low and high frequency range. Here, elastic, viscous and inertial couplings between air and the solid was modeled. Other models to predict micro- and macroscale acoustical parameters of porous materials have developed. Miki [41] (an extended work of Delany and Bazley), Attenborough [42] (an influence of tortuosity and the geometry of pores at high frequency), Johnson et al. [10] (a behavior of a Newtonian fluid subjected to a pressure gradient in porous media and the concept of dynamic tortuosity and permeability) and Champoux and Allard [11] (the thermal exchanges of the boundary layers

between the air saturated material and the wall of pores in porous media) were the precedents for the empirical and analytical models.

In order to predict and evaluate the sound absorption performance according to the microstructure of cell in porous media, a multiscale modeling is performed based on the finite element method (FEM) using the acoustic module in COMSOL Multiphysics software. Here, periodic unit cells (PUC's), a replicate of cell microstructure, and Johnson-Champoux-Allard (JCA) model, a well-known simplest model for sound propagation over a wide range of frequency, were used. This JCA model is based on identifying five intrinsic properties of the porous medium. First, porosity (ϵ_p) and thermal characteristic length (TCL, L_{th}) are directly derived from the PUC's. And other parameters, *i.e.* flow resistivity (R_f), viscous characteristic length (VCL, L_v), and tortuosity (τ_∞) can be obtained from the two (micro- and macroscale) flow analyses.

First, in microscale flow analysis, a viscous flow problem is solved using Stokes' equation with the following boundary conditions [24, 43-46]

$$\mu\nabla^2\boldsymbol{v} - \nabla p = \boldsymbol{g} \text{ in } \Omega_\mathrm{f} \tag{2}$$

$$\nabla \cdot \boldsymbol{v} = 0 \text{ in } \Omega_\mathrm{f} \tag{3}$$

$$\boldsymbol{v} = 0 \text{ on } \Omega_\mathrm{sf} \tag{4}$$

where μ is the viscosity of air, $\boldsymbol{v}$ is the velocity field, p is the pressure, $\boldsymbol{g}$ is the constant vector field of pressure gradient around the fluid domain, Ω_f is the fluid domain, and Ω_sf is the boundary of the solid-fluid interface. The velocity vector field ($\boldsymbol{v}$) is obtained from the Eqs. 2-4. And the permeability field is attained by input the velocity field into the following equation, $\boldsymbol{k_0} = -\mu\boldsymbol{v}/|\boldsymbol{g}|$ where $\boldsymbol{g}$ is the pressure gradient (Pa/m), a constant throughout the whole fluid domain of the PUC. Then, the flow resistivity (R_f) is acquired by

$R_f = \mu/(< \boldsymbol{k_0} >_f \cdot \epsilon_p)$, where ϵ_p is the porosity, and $< \boldsymbol{k_0} >_f \cdot \epsilon_p$ is the permeability value in a porous medium, where $\boldsymbol{k_0}$ is the permeability of the averaged PUC over the whole fluid domain.

Second, an inertial flow problem almost behaves like incompressible-inviscid ideal flow problem [47]. Thus, this problem can be altered to an electrical conduction (Laplace problem) with the following boundary conditions [24, 46].

$$\boldsymbol{E} = -\nabla\varphi + \boldsymbol{e} \text{ in } \Omega_\mathrm{f} \tag{5}$$

$$\nabla \cdot \boldsymbol{E} = 0 \text{ in } \Omega_\mathrm{f} \tag{6}$$

$$\boldsymbol{E} \cdot \boldsymbol{n} = 0 \text{ on } \Omega_\mathrm{sf} \tag{7}$$

where $\boldsymbol{E}$ is the scaled electric field, $\nabla\varphi$ is the fluctuating part with the scalar field φ, and $\boldsymbol{e}$ is the unit vector field [43]. Tortuosity and the viscous characteristic length can be obtained by inserting the obtained scaled electric field from Eqs. 4-6, $\tau_\infty = < \boldsymbol{E}^2 >_\mathrm{f} / < \boldsymbol{E} >_\mathrm{f}^2$ and $L_v = 2\int_{\Omega_\mathrm{f}} \boldsymbol{E}^2 \, \mathrm{d}\Omega_\mathrm{f} / \int_{\Omega_\mathrm{sf}} \boldsymbol{E}^2 \, \mathrm{d}\Omega_\mathrm{sf}$ [46]. For thermal characteristic length (L_{th}), an estimation of a hydraulic radius of the PUC is evaluated by $L_{th} = 2\int_{\Omega_\mathrm{f}} \mathrm{d}\Omega_\mathrm{f} / \int_{\Omega_\mathrm{sf}} \mathrm{d}\Omega_\mathrm{sf}$. By using two flow problems with five poroacoustic parameters, the JCA model can be calculated for the frequency-dependent complex variables, effective bulk density ($\rho(\omega)$) and effective bulk modulus (K(ω)).

$$\rho(\omega) = \frac{\tau_\infty \rho_f}{E_p}\left(1 + \frac{R_f \epsilon_p}{\mathrm{i}\omega\rho f \tau_\infty}\sqrt{1 + \frac{4\mathrm{i}\omega\tau_\infty^2 \mu \rho_f}{R_f^2 L_v^2 E_p^2}}\right) \tag{8}$$

$$K(\omega) = \frac{\gamma_f P_A}{\epsilon_p}\left[\gamma_f - (\gamma_f - 1)\left(1 + \frac{8\mu}{\mathrm{i}\omega L_{th}^2 Pr \rho_f}\sqrt{1 + \frac{\mathrm{i}\omega\rho_f P_r L_{th}^2}{16\mu}}\right)^{-1}\right]^{-1} \tag{9}$$

where ρ_f is the density of air, ω is the angular frequency, γ_f is the heat capacity of air, P_A is the ambient pressure, Pr is Prandtl number, and μ is the viscosity of air.

The values obtained from Eqs. 8-9 are substituted into Eqs. 1 and a 2-D replica of B&K impedance tube is designed using a pressure acoustics module in COMSOL Multiphysics software. The replica was composed of a perfectly matching layer, air domain, and foam domain (Fig. 7). The bottom and the lateral walls were set to the sound hard boundary condition and the air domain as a linear elastic fluid. The dimension of the foam domain was adjusted to match the same size of the experimental sample cuts (29 mm diameter and 20 mm height by each). Using the pressure acoustics module, the normal incident background pressure field was found to be $p_i = \exp(-\mathrm{i}(k \cdot x))$, where p_i is the incident wave pressure, k is the wave number. The range of frequency measured in the background field was from 0 to 6400 Hz in a plane wave condition. With an integration of all acoustical parameters, $\rho(\omega)$, $\beta(\omega)$ and p_i with Eqs. 1, a simple Helmholtz equation (S.H.E.), scattered pressure fields (p_s) and total pressure fields (p_t) can be obtained by $p_t = p_i + p_s$. Last, the final result, sound absorption coefficient (α), was obtained; $\alpha = 1 - |R|^2$, where $R = p_s/p_i$.

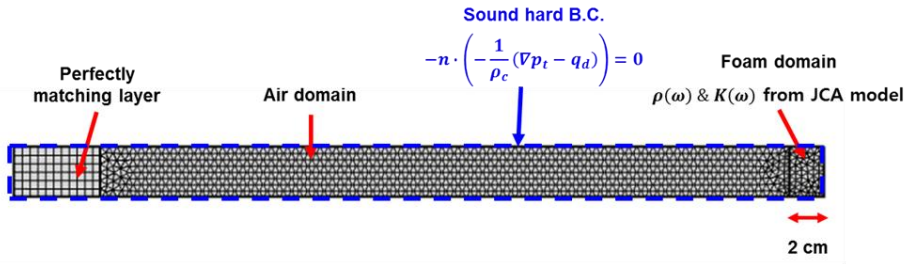

Figure. 7 A replica design capture of a real B&K impedance tube in COMSOL Multiphysics.

Chapter 3. Experimental Method

3.1 Materials

Reactant A, two kinds of polyols (NIXOL SA-120, NIXOL RNF-180, KPX Chemical, Republic of Korea), and Reactant B, 4,4‘-diphenylmethane diisocyanate (MDI, MCNS, Republic of Korea), were prepared. And poly(ethylene glycol) 2000 (PEG 2000, Mw = 2000, DAEJUNG Chemical, Republic of Korea) as a reactive cell opening agent was used. A releasing agent (AKO-HM207K, Akochem, Republic of Korea) was also prepared for easy and clean mould release. Detailed information is listed in Table 3.1.

3.2 Fabrication of Semi-open Cell Polyurethane Foam

Before the polymerization reaction involving the polyol and the isocyanate, PEG 2000 was added to the reactant A (NIXOL SA-120 : NIXOL RNF-180, 3:1 mixing ratio) for the variation of cell openness with different weight percentage by 0, 3, 6 wt%. The reactant A, with the addition of PEG 2000, was agitated for overall uniform dispersions of PEG using a digital regulator (WiseStir® model HS-100D, Germany) at 3000 rpm for 30 min. After the agitation, the modified reactant A and the reactant B were rapidly mixed together in a ratio of 1:1 in a lab-made plastic cup using the same regulator at 3000 rpm for 5 seconds. Once cream time, gel time and rise time are checked, the mixture of the reactant A and B was poured into the mould (15 x 15 x 2 cm^3). The mould was designed and prepared to maintain an identical density (40 kg/m^3) and thickness of the fabricated foams (Fig. 8). Each fabricated samples were named after different weight percentage of PEG 2000; P0, P3, and P6.

Table 3.1
Materials used for the experiments

Material	Description	
Polyol (KPX Chemical) (K1/K2 mix ratio = 3:1)	K1 (NIXOL SA-120) Polyether polyol (94%)	K2 (RNF-180) Polyether polyol (40%)
Isocyanate (MCNS)	Diphenylmethane 4,4'-diisocyanate (MDI)	
Blowing Agent	Water (2.3%)	Water (20%)
Other Components	Surfactant Catalyst	TCPP (Flame retardants : 40%) Polysiloxanes (2%) S1, S2 (Confidential)
Cell Opening Agent (DAEJUNG Chem.)	Poly(ethylene glycol) 2000, Mw = 2000	
Mold Releasing Agent (Akochem)	AKO-HM207K	

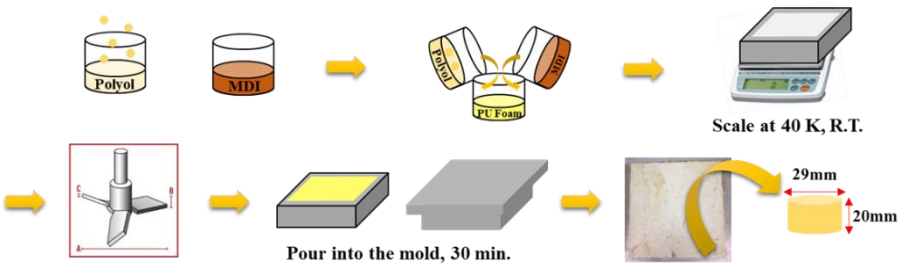

Figure. 8 Experimental procedures of polyurethane foam fabrication with the addition of PEG 2000

3.3 Microcellular Morphology

The fabricated foams were cut into small specimens and dipped into N_2 liquid using a freeze-cut-drying method before SEM observation. Cell diameter and cell openness of the specimens were observed through images using a field emission scanning electron microscope (MERLIN Compact FE-SEM, ZEISS, Germany). These two parameters were more precisely analyzed using Image-Pro Plus 6.0 software based on porosimetry calculation. The total mean diameter of the sample was calibrated by the ratio of pixel size and the average cell diameter of cells in the taken SEM images [24]. The cell diameter was defined as the average value of the length of short and long axis of a cell. Cell openness (p) was defined as $p = S_{open}/S_{total}$, where S_{open} is the open area and S_{total} is the total area of cell walls [27].

3.4 Sound Absorption Coefficient Measurement

Impedance tube kit (50 Hz – 6.4 kHz) type 4206, a Brüel & Kjaer (B&K) impedance tube was used based on the two-microphone transfer function method according to ISO 10534-2 and ASTM E 1050-12 ([48] and (Fig. 9). The B&K impedance tube was supported by a grant from Prof. Yeon June Kang, Institute of Advanced Machinery and Design Lab, Department of Mechanical Engineering, Seoul National University, Korea. Normal incidence absorption coefficient and the sound pressure at two microphones can be measured. To obtain the normal incidence absorption coefficient, the sound pressure of each two microphone is positioned by,

$$P_1 = \left(Ae^{-jkx_1} + Be^{jkx_1}\right)e^{j\omega t} \quad (10)$$

$$P_2 = \left(Ae^{-jkx_2} + Be^{jkx_2}\right)e^{j\omega t} \quad (11)$$

where A and B represent the amplitude of incident wave and reflected wave in the tube respectively, k is the wavenumber, and x_1 and x_2 are the distances from the sample to each microphone 1 and 2. The transfer function which is the sound pressure ratio of each two microphone is represented by

$$H_{12} = \frac{P_1}{P_2} = \frac{Ae^{-jkx_1} + Be^{jkx_1}}{Ae^{-jkx_2} + Be^{jkx_2}} = \frac{e^{-jkx_1} + Re^{jkx_1}}{e^{-jkx_2} + Re^{jkx_2}} \quad (12)$$

where R is the reflection coefficient which is the ratio of A and B. The reflection coefficient is expressed by the transfer function, H_{12} by following equation.

$$R = \frac{-e^{-jkx_1} + H_{12}e^{-jkx_2}}{e^{jkx_1} - H_{12}e^{jkx_2}} \quad (13)$$

The sound absorption coefficient (α) is calculated through the reflection coefficient obtained from Eqs. (13).

$$\alpha = 1 - |R|^2 \quad (14)$$

Then the final outcome, the sound absorption coefficient, was defined as $\alpha = 1 - |R|^2$, a value between 0 and 1 and if the value is close to 1 meaning well-absorbed sound energy.

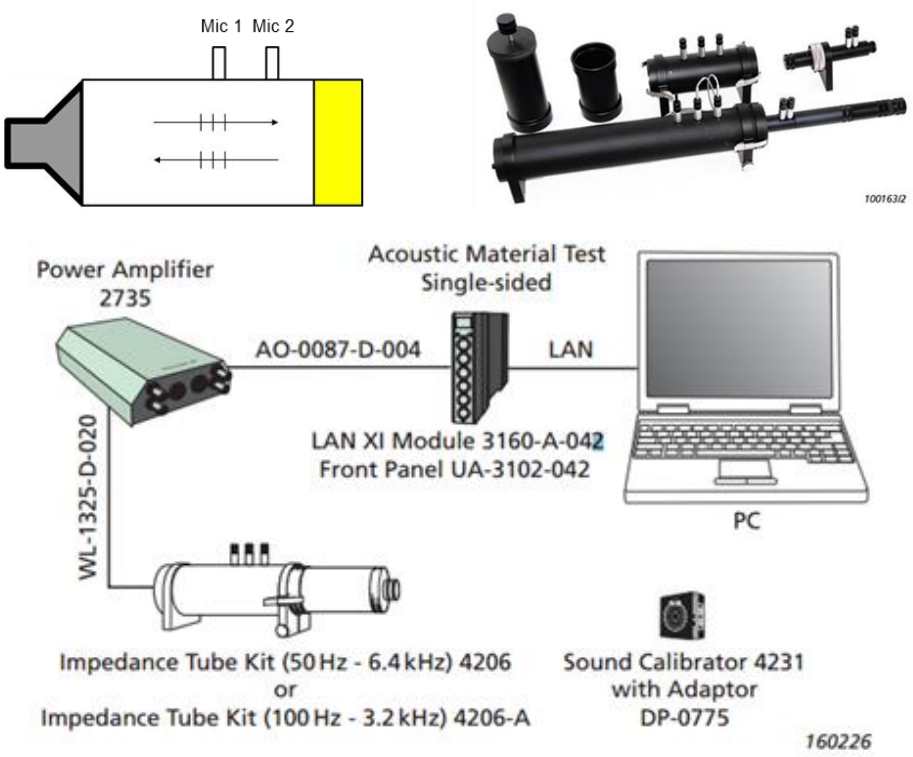

Figure. 9 B&K impedance tube for sound absorption coefficient by ASTM 4206 [48]

3.5 Tortuosity Measurement

A lab-made electrical conductivity measurement was designed for measuring tortuosity (τ_∞). The set up was made by the following reference, which was also designed schematically [49]. Electrical resistance of a conductive fluid (Ω_f), NaCl and a fluid-saturated foam resistance (Ω_m) were considered for a function of $\tau_\infty = \varepsilon \cdot (\Omega_m/\Omega_f)$, where ε is the porosity.

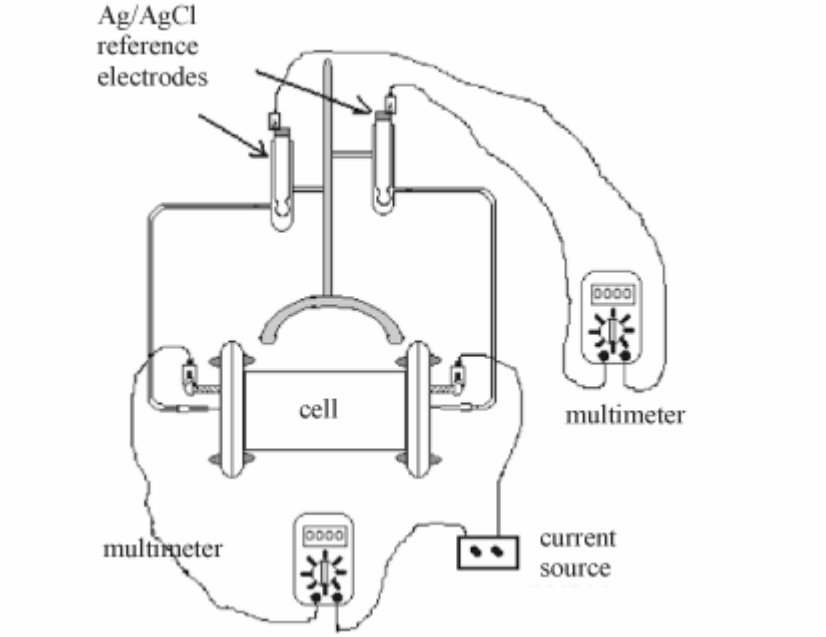

Figure. 10 Diagram of the equipment for the tortuosity measurements [49]

Chapter 4. Results & Discussion

As noted earlier, cell openness manipulation is considered to be one of the most influential methods in enhancing the sound absorption performance in porous sound absorber. A polyurethane foam (PUF) is normally classified into open cell, closed cell, and semi-open cell by the morphology of the foam. For the open cell foam, a sound wave penetrates through a porous medium with bare obstacles due to the hollow and less complex path of the foam microstructure. On the other hand, for the closed cell structure, the sound wave cannot penetrate and is reflected by the surface of the foam instead. So, it can be called 'sound insulation' instead of 'sound absorption.' In this study, the optimal cell openness condition for the experimental method and the numerical approach of semi-open cell foam is suggested.

4.1 Experimental Results

SEM images of PUF sample P0, P3, and P6 (different wt % addition of PEG 2000) were obtained (Fig. 11 (a-d)). First, P0 sample was fully-closed cell structure (Fig. 11 (a)). There was no PEG 2000 mixed with the polyol mixture and cell windows or walls were almost closed. Sound waves could not penetrate into the microstructure of P0 sample. Figure 11. (b-c) demonstrated how PEG 2000, a cell opening agent, generated pores from closed cell to semi-open cell structure PUF. The display of P6 sample seemed to contain more pores than those of P3 sample in SEM images.

Previously mentioned, cell openness (p) was calculated by $p = S_{open}/S_{total}$, where S_{open} is the open area and S_{total} is the total area of cell walls. Respectively, P3 and P6 sample were confirmed to have an estimation of

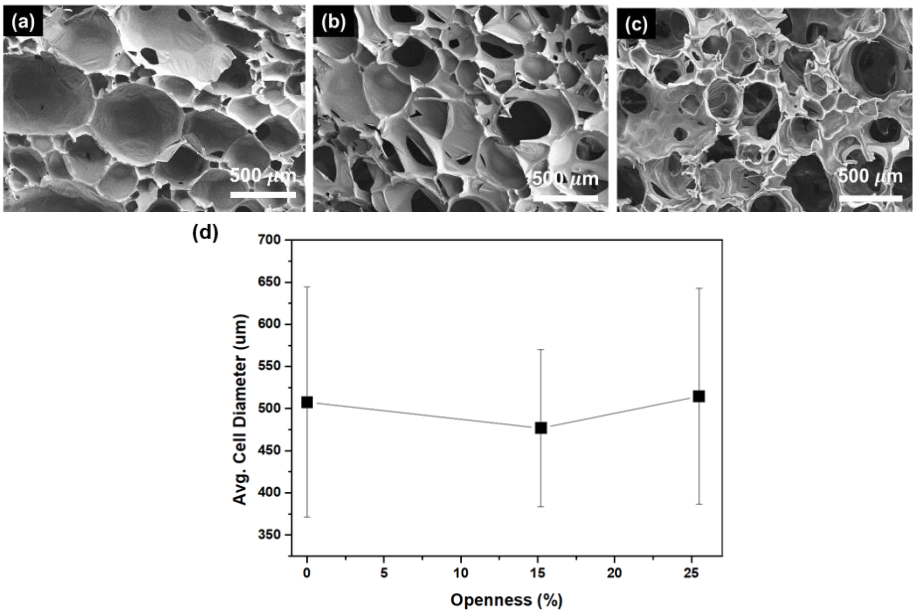

Figure 11. (a-c) SEM images of the fabricated samples, P0 (0% openness), P3 (15% openness), and P6 (22% openness) and (d) cell size distribution of the samples.

around 15% and 22% cell openness using Image-Pro Plus 6.0 software based on porosimetry calculation. For the verification of uniform cell size distribution, the specific dimension of each sample was measured, 507±130 μm (P0), 478±93 μm (P3), and 515±128 μm (P6) (Fig. 11 (d)). Since there was a small margin of error in the cell size, it turned out that cell openness was considered more importantly for the sound absorption coefficient measurement. Unfortunately, much higher percentages of PEG 2000 could not be attempted due to the imbalance of chemical reaction, cell rupture or collision according to the cell opening mechanism. Even P6 sample had difficulties such as a rough strut shape and defects in fabrication. Also, less than 15% cell openness (P3) sample was not able to be produced because there was no remarkable change of pores by adding less than 3 wt% of PEG 2000. Hence, 0% (P0), 15% (P3), and 22% (P6) cell openness samples were fabricated ultimately; and the sound absorption performance of these samples were compared with the numerical simulation results.

4.2 Unit Cell Modeling

For an idealized foam microstructure, a construction of periodic unit cells (PUC's) was developed by CATIA (Computer Aided Three-dimensional Interactive Application) software. A "tetrakaidecahedron" cell structure, particularly known as Kelvin cell, has been used for the foam model. This theoretical approach has shown good correlation with the real PU foam structure in several cases [50-53]. First, 15 tetrakaidecahedrons were attached to create a cluster which represent microscale pore structure of the unit cells (Fig. 12 (a)). An elimination of cell windows were randomly selected by the random number generation function using MATLAB software for each different cell openness PUC's (Fig. 12 (b)). Importing a hexahedron, which has repetitive faces in every direction, into the cluster (Fig. 12 (c)), a Boolean

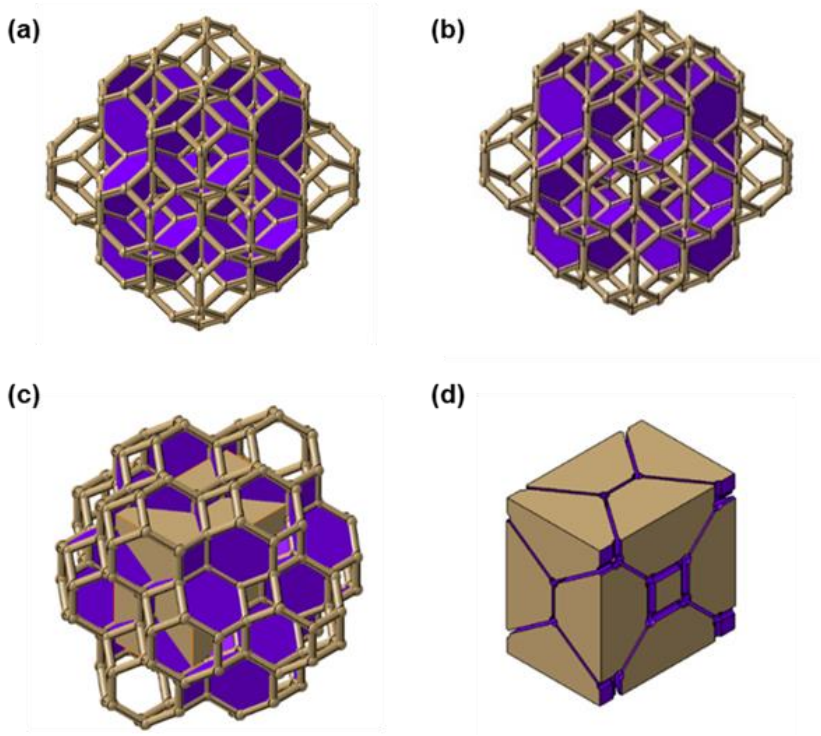

Figure. 12 (a) A monodispersed cluster of 15 tetrakaidecahedron, (b) An elimination of cell windows, (c) Importing a hexahedron into the cluster, (d) A Boolean operation of PUC's

operation in CATIA software was applied to subtract or remove those overlapped faces or sides of the PUC's (Fig. 12 (d)). All PUC's were identical in design *e.g.* cell density (40 K (=kg/m^3)) and cell size (500μm), which were same with the experimental results.

Next, each different cell openness PUC's were designed; 15, 25, 50, 100% (Fig. 13 (a-d)). The openness of cell windows was determined by the ratio of opened cell windows to the total number of cell windows, which was a similar method referred to the correlation between the acoustic and porous cell morphology of PUF [27]. Considering the lateral surface of the PUC in periodic boundary condition, the flow analysis is solved with the elimination of center cell walls. For example, 15% cell openness of PUC had a removal of 2 rectangles and 2 hexagons at the center cell; 25% cell openness (removal of 3 rectangles and 4 hexagons); 50% cell openness (removal of half of PUC, 6 rectangles and 8 hexagons). For 100% cell openness, only the cell struts or walls were remained as a fully open cell structure.

4.3 Multiscale Poroacoustics Simulation

Multiscale poroacoustic simulation was performed using four different periodic unit cells (PUC's); 15, 25, 50, and 100% cell openness. As previously mentioned, Johnson Champoux Allard (JCA) model with five acoustical parameters (ϵ_p, L_{th}, R_f, L_v, τ_∞) were obtained from viscous and inertial flow problems. Again, the numerical simulation was run by using the acoustic module in COMSOL Multiphysics software based on finite element method (FEM) [9,46]. Here, porosity was fixed to 0.96 from the implemented PUC structure.

First, in microscale flow analysis, viscous flow problem was solved in order to derive flow resistivity in the PUC. Assumptions were applying period boundary condition on the lateral surfaces of the PUC with no-slip

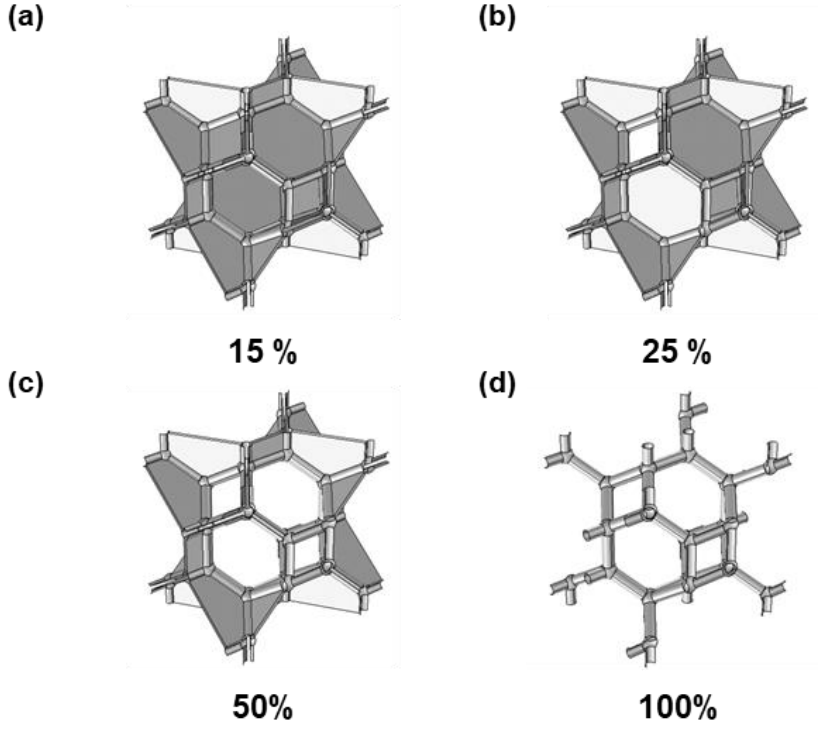

Figure. 13 A construction of four different periodic unit cells (a) 15%, (b) 25%, (c) 50%, (d) 100%

boundary condition on the solid-air interface and pressure boundary condition on the PUC surface in z-direction. Solving Stokes' flow equation, the value of permeability fields ($\boldsymbol{k_0}$) was obtained and the scaled velocity fields considering the viscosity of air were determined. Then, the flow resistivity (R_f) of each PUC was computed with input value from the scaled velocity profile and porosity (0.96).

Second, tortuosity and viscous characteristic length (VCL) were derived by solving electrical current conservation equation. In a similar manner, scaled electric fields ($\boldsymbol{E}$) were obtained assuming potential boundary condition on the PUC surface in z-direction with the periodic boundary condition. Both scaled velocity and electric fields were described in (Fig. 14. a-d). Cell openness of 15% PUC appeared to have the most complex inner structure compared to other three different (25, 50 and 100% cell openness) PUC's. From figure 14. (a), streamlines, multiple red curves, for 15% cell openness PUC were tilted and tangled the most. This can be interpreted as cell openness of the PUC's decreases, more complex inner paths of PUC's are generated. In other words, tortuosity parameter is increased as the degree of cell openness is decreased (Table. 4.3 & Fig. 20). The calculated values were 3.7 (15% cell openness PUC), 2.0 (25% cell openness PUC), 1.4 (50% cell openness PUC), and 1.02 (100% cell openness PUC).

Now, the simulation for pressure acoustics, macroscale analysis, using JCA model was executed to investigate the sound wave propagation behavior of PUC's. Since the noise generated by vehicles are gathered in the frequency range at 1,000 and 2,000 Hz, results were obtained at 1,000 Hz and 2,000 Hz with background and scattered pressure fields (Fig. 15 (a-d)). Each leftmost B&K impedance tube imitation demonstrates the background pressure fields with no sound absorbing domain and the rests (15, 25, 50, and 100% cell openness PUC) were the scattered pressure fields with sound absor-

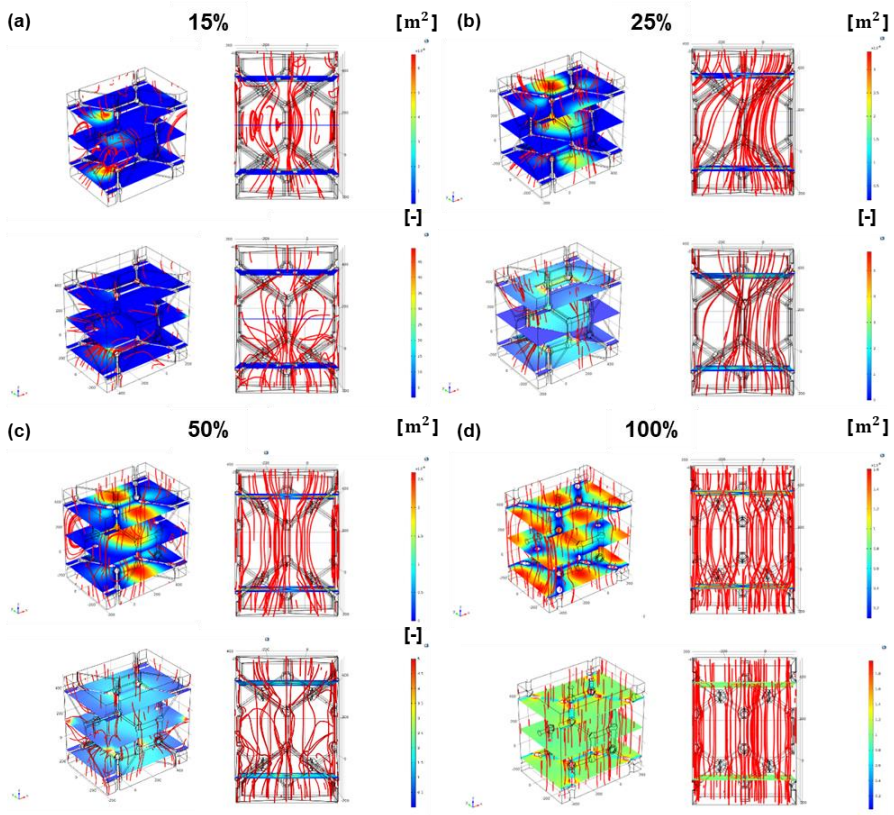

Figure. 14. Solutions of viscous (top for each) and inertial (bottom for each) flow problem in microscale numerical analysis using each different PUC's (a) 15%, (b) 25%, (c) 50%, and (d) 100% cell openness PUC.

Table 4.3
Calculated poroacoustics parameters

Cell Openness	15%	25%	50%	100%
ϵ_p	0.96	0.96	0.96	0.96
τ_∞	3.7	2.0	1.4	1.02
R_f $(N \cdot m^4 \cdot s)$	4620	3100	2738	2326
L_v (μm)	80	138	159	301
L_{th} (μm)	165	174	231	516

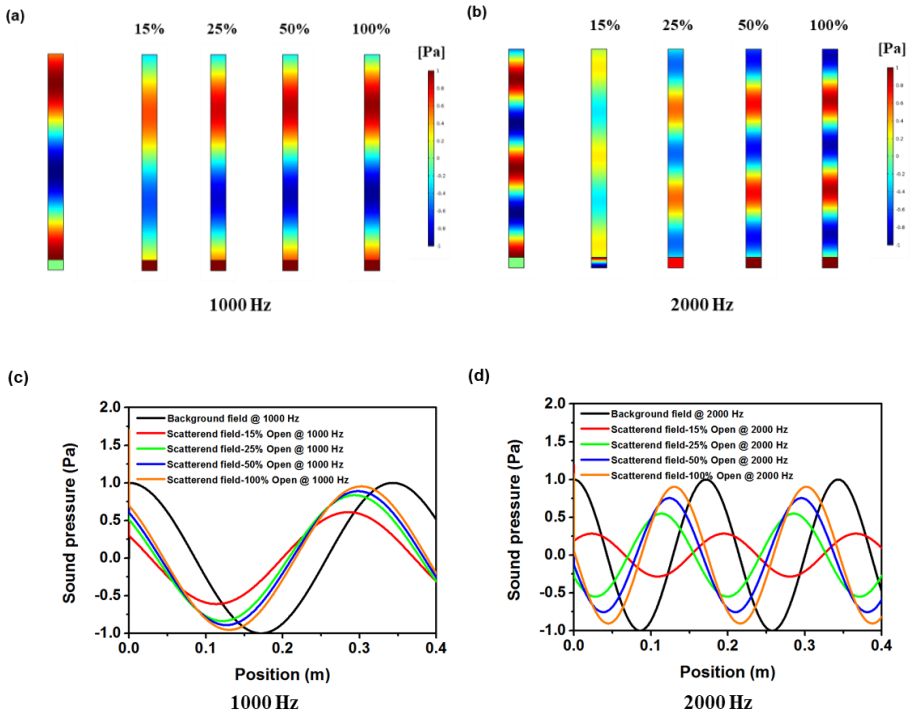

Figure. 15. Macroscale pressure acoustics simulation results at (a) 1,000 Hz, (b) 2,000 Hz for each different cell openness PUC's. The profiles of sound pressure field in the tube for each PUC in background and scattered pressure fields (c) at 1,000 Hz and (d) at 2,000 Hz.

-bing domain from left to right. Figure. 15 (c-d) reveal the profiles of sound pressure field in the tube for each different PUC at 1,000 Hz and 2,000 Hz. Likewise, the intensity of scattered pressure fields in 15% cell openness PUC had superior sound damping efficiency compared to other PUC's. Also, the degree of cell openness was proportional to the damping efficiency.

JCA model is composed of two frequency-dependent complex variables, $\rho(\omega)$ and $K(\omega)$. The relationship between cell openness and the sound wave propagation was confirmed that the decrease in cell openness value induces an increase in tortuosity parameter, but the decrease in two characteristic lengths (L_v and L_{th}) (Table 4.3). Figure 16. (a-c) shows two complex variables of air in porous domain for each PUC. From Eqn. 8, tortuosity increase and decrease L_v affect large value of effective density $\rho(\omega)$. On the other hand, the bulk modulus $K(\omega)$ is proportional to the L_{th} in Eqn. 9. A resistance of acoustic flow in medium, characteristic impedance (Z_c) proposed by Delany and Bazley [39], was implemented for the calculation of $Z_c = [K(\omega)\rho(\omega)]^{1/2}$ and complex phase speed (C_c), where $C_c = K(\omega)/\rho(\omega)$ which are reciprocal to each other (Fig. 16. (c)). Overall, $\rho(\omega)$ was gradually increasing with the lower degree of cell openness and $K(\omega)$ was decreasing with the opposite trend. In other words, large air density and small bulk modulus slow down the speed of sound wave in overall frequency range, but they become more influential in low frequency range.

4.4 Comparison of Experimental and Simulation Results

Both experimental and simulations results of all samples are shown in Figure. 17. P0 sample, which is a closed cell foam meaning non-existence of the inner path, had the lowest sound absorption coefficient, 0.2. The values of P6 sample (22% cell openness) curve were positioned between 15% and 25% cell

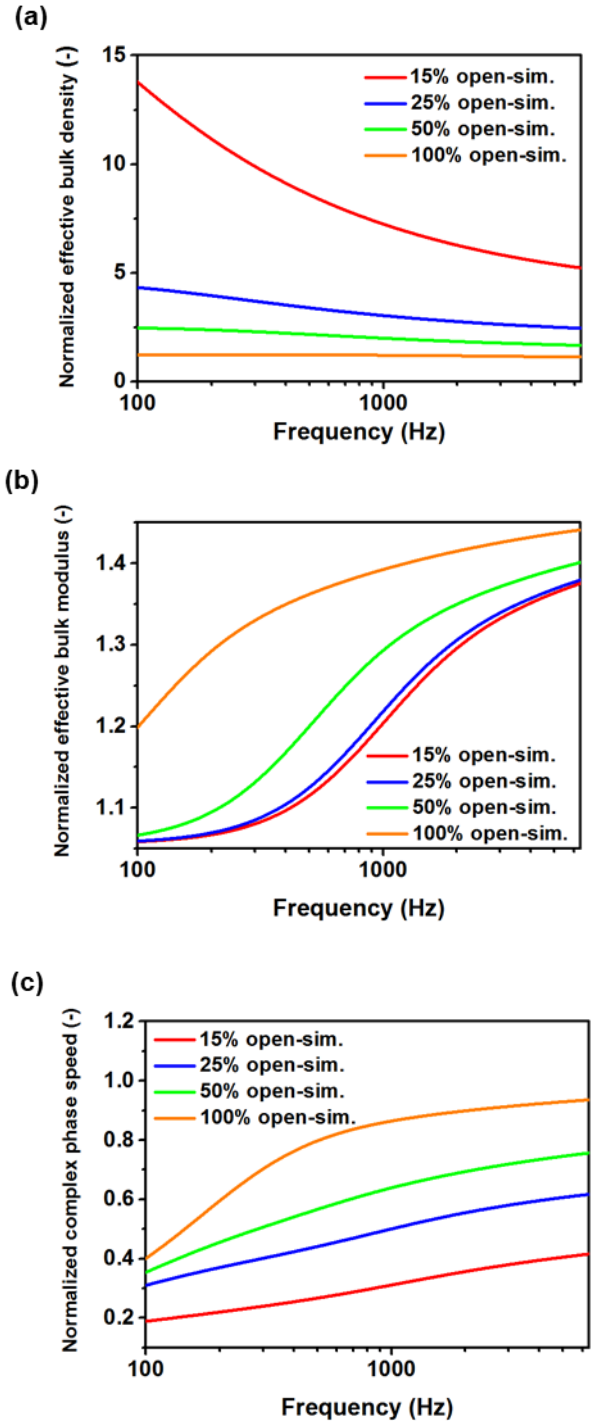

Figure. 16. Two frequency dependent **c**omplex variables, (a) effective bulk densitym, (b) effective bulk modulus, and (c) complex phase speed curves normalized with air properties.

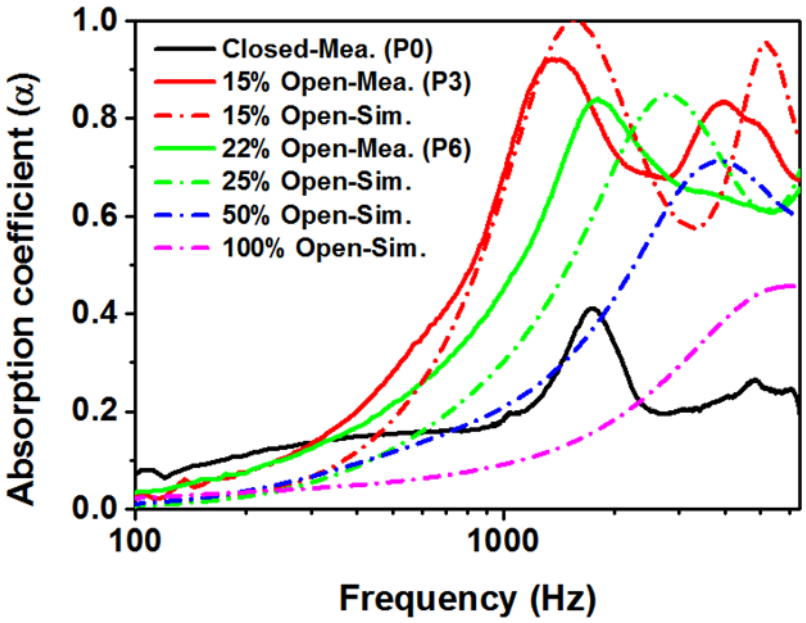

Figure. 17. Sound absorption coefficients of measured and simulation results

openness simulation results. It was clear to confirm that the P3 sample (15% cell openness) was shifted more toward lower frequency region compared to P6 sample. Even, the simulation results of 15% cell openness PUC almost corresponded well with the experimental result of P3 sample curve. The cell size (500 μm) of the two samples was almost the same. This proves that cell openness difference of PUC between two samples is the main reason for the mainpulation of sound absorbing behavior at low frequency.

For more quantitative sound absorption performance analysis, a root mean square (RMS) and a noise reduction coefficient (NRC) were conducted and compared with both measured and simulation results. RMS 2,000 value (range from 0 to 2,000 Hz), a major noise frequency range in automobiles, appeared to be decreased as cell openness increased (Fig. 18 (a)). And the P3 sample had the highest RMS 2,000 value among other samples. Second, NRC is the standard value for the evaluation of sound damping materials. It is the sum of the sound absorption coefficients at 128, 256, 512, 1,024, 2,048, and 4,096 Hz which is divided by the number of frequency added (Fig. 18 (b)). In other words, NRC is the average sound absorption coefficient over the wide frequency region. Third method, 1/3 Octave band spectrogram, is used for good standard for the audible frequency range for humans (Table 4.5). The spectrogram can be obtained by dividing measured frequencies into each band range. For example, one octave range with the highest frequency is higher twice as much compared to the lowest frequency. Fig. 19 (a-b) shows the octave bands of both measured and simulation results for the case of each cell openness. Most bands of the 15% openness PUC seems to have much higher sound absorption coefficients than other cases. All three analyses confirmed that the P3 sample is an excellent sound absorber and can efficiently eliminate most noises of major automobiles.

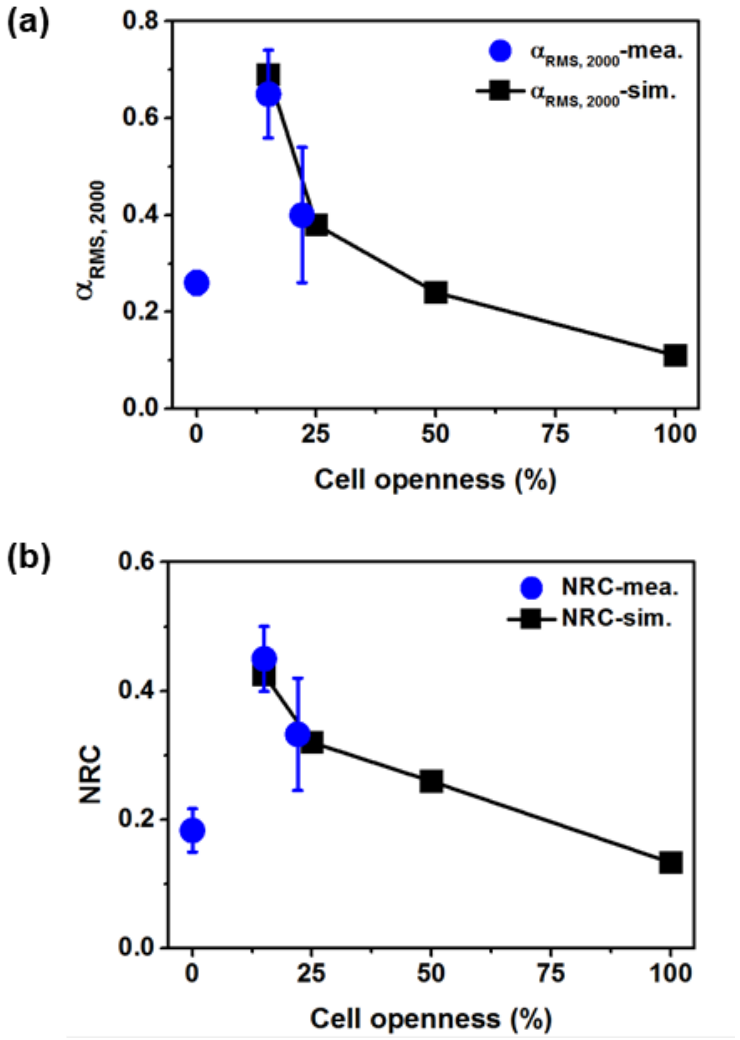

Figure. 18. Sound absorption performance (a) RMS values from 0-2,000 Hz vs. cell openness and (b) NRC values vs. cell openness

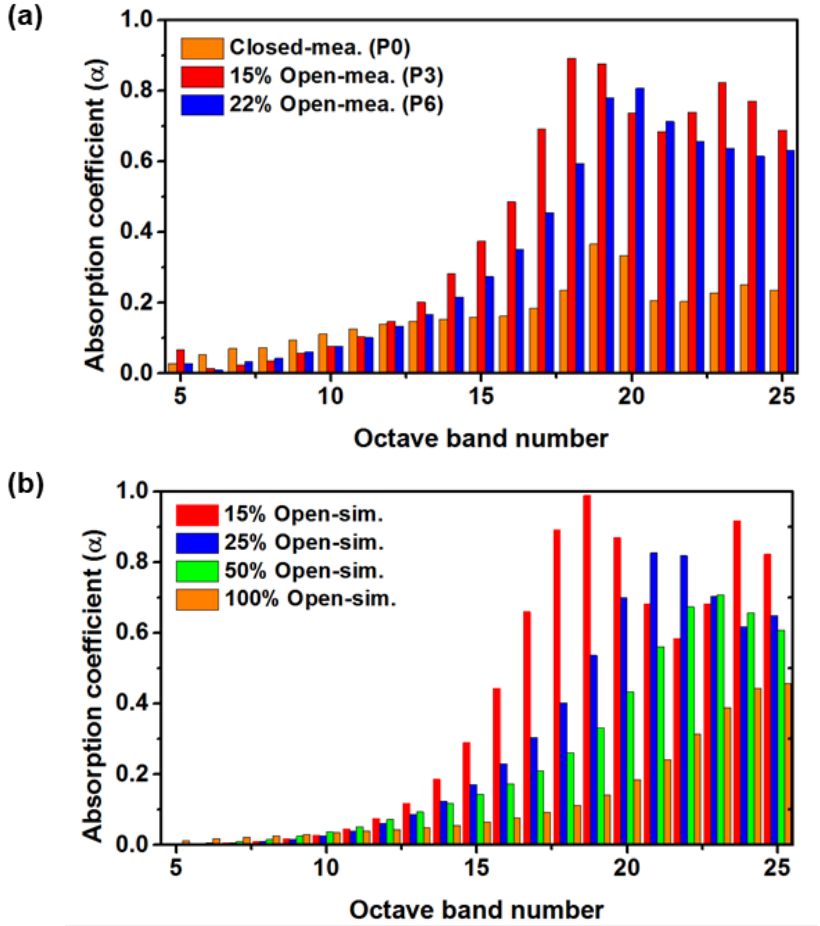

Figure. 19. 1/3 octave band data for (a) the measurement results and (b) the simulation results.

Table 4.4
Numbers of 1/3 octave band spectrogram for each band.

1/3 Octave band number	Center frequency of band (Hz)
1	25
2	31.5
3	40
4	50
5	63
6	80
7	100
8	125
9	160
10	200
11	250
12	315
13	400
14	500
15	630
16	800
17	1000
18	1250
19	1600
20	2000
21	2500
22	3150
23	4000
24	5000
25	6300

It was found out that tortuosity (τ_∞) of the measured and simulation results coincided in trend (Fig. 20). Due to the fabrication problem, only P3 (15% cell openness and P6 (22% cell openness) sample were measured through tortuosity measurement. The P3 sample has more complex cellular structure than P6 sample because of more closed cell regions inside. Thus, high value of tortuosity was obtained from the P3 sample. This also can be attributed to complex path of the sound wave propagation.

Comparing with other acoustical parameters, the sensitivity analysis of each PUC's varying tortuosity, two characteristic lengths (VCL and TCL, simultaneously), and flow resistivity was performed. The default parameter in this analysis was 100% openness PUC (Fig. 21). Still, sound damping efficiency of 15% openness PUC was mostly fluctuated at low frequency region, due to the narrow and complex sound propagating path in the foam.

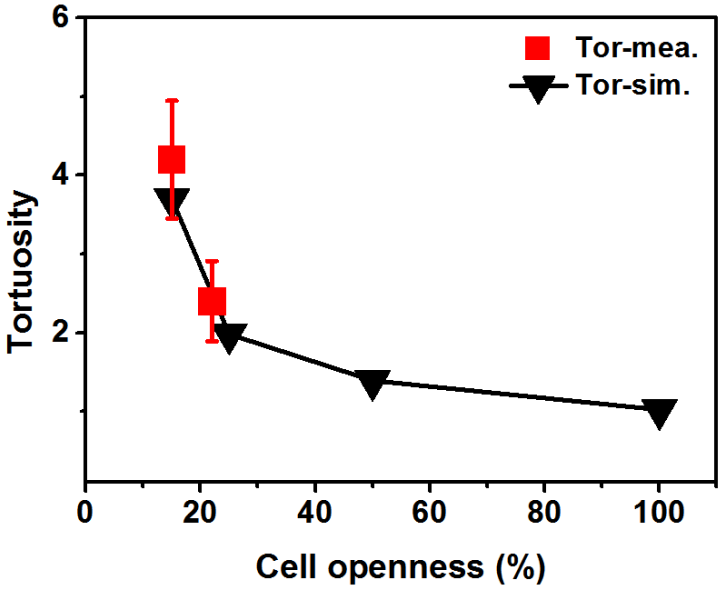

Figure 20. Sound absorption performances of measured and predicted tortuosity depending on cell openness.

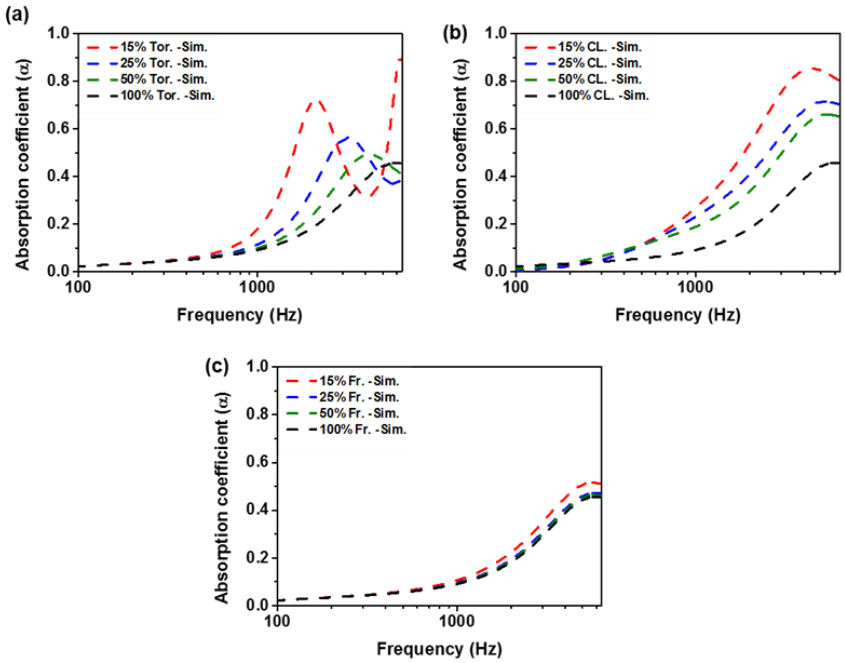

Figure 21. A sensitivity analysis for (a) tortuosity (Tor.), (b) characteristic lengths (VCL and TCL), and (c) flow resistivity (Fr.) for different cell openness PUC.

4.5 Feasibility of Low Density Polyurethane Foam

Commercial foam in auto industry has a mass density of 80 kg/m^3, double mass density of the 40 K. The sound absorption performance of the P3 sample is comparable with that of the commercial foam (Fig. 22 (a)). The maximum peak frequency of P3 sample was shifted close to 1,000 Hz range even with half number of density (40 kg/m^3). Moreover, RMS 2,000 and NRC values of the P3 sample had higher sound absorption coefficients compared to that of commercial foam (Fig. 22 (b-c)). Normally, a high density foam has a better chance of showing superior sound absorption performance due to its complex microcellular geometry. However in this research, the P3 sample alerted that optimizing cell openness provokes the outstanding sound absorption performance, showing the possibility of low density foam application in the automotive industry.

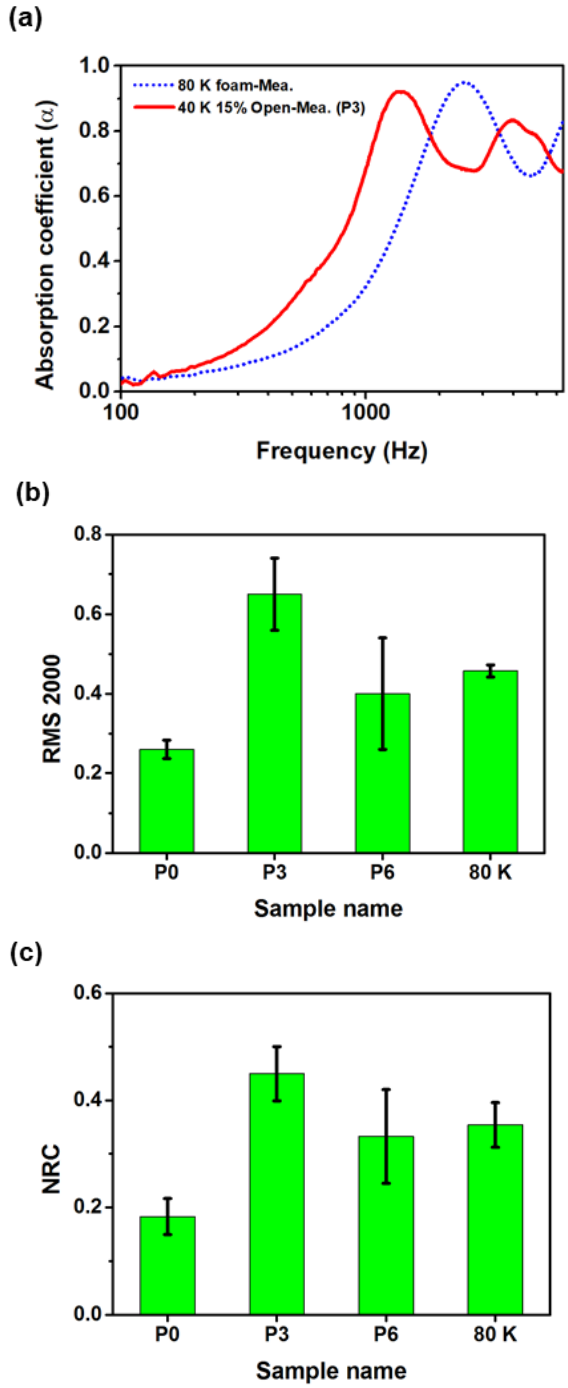

Figure 22. Comparison of sound absorption performances between P3 sample and 80 kg/m^3 commercial foam (a) sound absorption coefficient, (b) RMS values of sound absorption coefficients from 0-2,000 Hz, and (c) NRC values.

Chapter 5. Conclusion

In this study, the innovative strategy is proposed for overcoming the limitation of mass density of PUF sound absorber. Lightweight polyurethane foams with optimized cell openness were fabricated and sound absorption performance of the foams were measured. Cell openness manipulation was considered to be the influential factor in most noise frequency range in vehicle. To support this argument, the measured sound absorption coefficients were compared with simulation results. The addition of reactive chemical opening agent, polyethylene glycol (PEG) 2000, with polyol mixture facilitated the openness of the cell microstructure. The inclusion of 3wt % of PEG 2000 (15% cell openness) showed the optimal formation of cell structures with appropriate closed cell contents. Accordingly, simulation results of 15% cell openness PUC (periodic unit cell) was compared with the measured sample P3, which almost had same cell openness. For additional quantitative analyses, RMS, NRC and 1/3 octave band spectrogram values of the foam samples were evaluated for both measured and simulation results.

The best sound absorption performance semi-open cell foam, P3 sample, had 15% openness, 500 μm cell size, and the mass density of 40 kg/m^3. From both measured and simulation results, it was concluded that tortuosity was the most influential parameter among acoustic parameters due to complex inner path of the microstructure. Moreover, 40 K P3 sample with 15% cell openness can be a powerful alternative for the 80 K commercial PU foam in automobile as it presents superior acoustic performances despite the reduction in its mass density.

Bibliography

1. Lee, L. J.; Ottino, J. M.; Ranz, W. E.; Macosko, C. W., Impingement mixing in reaction injection molding. *Polymer Engineering & Science* **1980,** *20* (13), 868-874.

2. Tucker, C. L.; Suh, N. P., Mixing for reaction injection molding. I. Impingement mixing of liquids. *Polymer Engineering & Science* **1980,** *20* (13), 875-886.

3. Despois, J.-F.; Mortensen, A., Permeability of open-pore microcellular materials. *Acta Materialia* **2005,** *53* (5), 1381-1388.

4. Scott, R., The propagation of sound between walls of porous material. *Proceedings of the Physical Society* **1946,** *58* (4), 358.

5. Biot, M. A., Generalized theory of acoustic propagation in porous dissipative media. *The Journal of the Acoustical Society of America* **1962,** *34* (9A), 1254-1264.

6. Zarek, J. H. B., Sound absorption in flexible porous materials. *Journal of Sound and Vibration* **1978,** *61* (2), 205-234.

7. Bolton, J.; Shiau, N.-M.; Kang, Y., Sound transmission through multi-panel structures lined with elastic porous materials. *Journal of sound and vibration* **1996,** *191* (3), 317-347.

8. Sagartzazu, X.; Hervella-Nieto, L.; Pagalday, J., Review in sound absorbing materials. *Archives of Computational Methods in Engineering* **2007,** *15* (3), 311-342.

9. Hoang, M. T.; Bonnet, G.; Tuan Luu, H.; Perrot, C., Linear elastic properties derivation from microstructures representative of transport parameters. *The Journal of the Acoustical Society of America* **2014,** *135* (6), 3172-3185.

10. Johnson, D. L.; Koplik, J.; Dashen, R., Theory of dynamic permeability and tortuosity in fluid-saturated porous media. *Journal of*

fluid mechanics **1987,** *176*, 379-402.

11. Champoux, Y.; Allard, J. F., Dynamic tortuosity and bulk modulus in air-saturated porous media. *Journal of applied physics* **1991,** *70* (4), 1975-1979.

12. Lafarge, D.; Lemarinier, P.; Allard, J. F.; Tarnow, V., Dynamic compressibility of air in porous structures at audible frequencies. *The Journal of the Acoustical Society of America* **1997,** *102* (4), 1995-2006.

13. Biot, M. A., Theory of propagation of elastic waves in a fluid-saturated porous solid. I. Low-frequency range. *The Journal of the acoustical Society of america* **1956,** *28* (2), 168-178.

14. Cotgreave, T.; Shortall, J., The mechanism of reinforcement of polyurethane foam by high-modulus chopped fibres. *Journal of Materials Science* **1977,** *12* (4), 708-717.

15. Cao, X.; Lee, L. J.; Widya, T.; Macosko, C., Polyurethane/clay nanocomposites foams: processing, structure and properties. *Polymer* **2005,** *46* (3), 775-783.

16. de Mello, D.; Pezzin, S. H.; Amico, S. C., The effect of post-consumer PET particles on the performance of flexible polyurethane foams. *Polymer Testing* **2009,** *28* (7), 702-708.

17. Javni, I.; Zhang, W.; Karajkov, V.; Petrovic, Z.; Divjakovic, V., Effect of nano-and micro-silica fillers on polyurethane foam properties. *Journal of cellular plastics* **2002,** *38* (3), 229-239.

18. Verdejo, R.; Stämpfli, R.; Alvarez-Lainez, M.; Mourad, S.; Rodriguez-Perez, M.; Brühwiler, P.; Shaffer, M., Enhanced acoustic damping in flexible polyurethane foams filled with carbon nanotubes. *Composites Science and Technology* **2009,** *69* (10), 1564-1569.

19. Gonzalez, A.; Ferrer, M.; De Diego, M.; Pinero, G.; Garcia-Bonito, J., Sound quality of low-frequency and car engine noises after active noise control. *Journal of Sound and Vibration* **2003,** *265* (3), 663-679.

20. Yamashita, T.; Suzuki, K.; Nishino, S.; Tomota, Y., Relationship between sound absorption property and microscopic structure determined by X-ray computed tomography in urethane foam used as sound absorption material for automobiles. *Materials transactions* **2008,** *49* (2), 345-351.

21. Youn, J., Processing of cellular polyurethane by ultrasonic excitation. *Journal of engineering for industry* **1992,** *114*, 323.

22. Cho, W.; Park, H.; Youn, J., Ultrasonic bubble nucleation in reaction injection moulding of polyurethane. *Proceedings of the Institution of Mechanical Engineers, Part B: Journal of Engineering Manufacture* **1994,** *208* (2), 121-128.

23. Park, H.; Youn, J. R., Study of reaction injection molding of polyurethane microcellular foam. *Polymer Engineering & Science* **1995,** *35* (23), 1899-1906.

24. Park, J. H.; Yang, S. H.; Lee, H. R.; Yu, C. B.; Pak, S. Y.; Oh, C. S.; Kang, Y. J.; Youn, J. R., Optimization of low frequency sound absorption by cell size control and multiscale poroacoustics modeling. *Journal of Sound and Vibration* **2017,** *397*, 17-30.

25. Tulliani, J. M.; Montanaro, L.; Bell, T. J.; Swain, M. V., Semiclosed-Cell Mullite Foams: Preparation and Macro-and Micromechanical Characterization. *Journal of the American Ceramic Society* **1999,** *82* (4), 961-968.

26. Guan, D.; Wu, J. H.; Wu, J.; Li, J.; Zhao, W., Acoustic performance of aluminum foams with semiopen cells. *Applied Acoustics* **2015,** *87*, 103-108.

27. Zhang, C.; Li, J.; Hu, Z.; Zhu, F.; Huang, Y., Correlation between the acoustic and porous cell morphology of polyurethane foam: Effect of interconnected porosity. *Materials & Design* **2012,** *41*, 319-325.

28. Yuge, K.; Muramatsu, H.; Masuda, Y.; Uekado, K.; Tanimoto, Y.,

Production and use of open cell rigid polyurethane foam. Google Patents: 1994.

29. Ahn, W., Open-Cell Rigid Polyurethane Foam Using Reactive Cell Opening Agents. *Journal of the Korea Academia-Industrial cooperation Society* **2013,** *14* (5), 2524-2528.

30. Song, K.; Lee, S.; Lee, D., Cell opening of high resilience polyurethane foam I. Concentration effect of polyether type cell opener. *Polymer-Korea* **2001,** *25* (5), 679-690.

31. Lee, S.-T.; Ramesh, N. S., *Polymeric foams: mechanisms and materials*. CRC press: 2004.

32. Frisch, K. C.; Saunders, J. H., *Polyurethanes; Chemistry and Technology*. John Wiley & Sons: 1964.

33. Frye, G. C.; Berg, J. C., Mechanisms for the synergistic antifoam action by hydrophobic solid particles in insoluble liquids. *Journal of colloid and interface science* **1989,** *130* (1), 54-59.

34. Neff, R. A. Reactive processing of flexible polyurethane foam. University of Minnesota, 1995.

35. Zhang, X.; Macosko, C.; Davis, H.; Nikolov, A.; Wasan, D., Role of silicone surfactant in flexible polyurethane foam. *Journal of Colloid and Interface Science* **1999,** *215* (2), 270-279.

36. Herrington, R.; Hock, K., *Flexible polyurethane foams*. Dow Chemical: 1997.

37. Kirchhoff, G., Ueber den Einfluss der Wärmeleitung in einem Gase auf die Schallbewegung. *Annalen der Physik* **1868,** *210* (6), 177-193.

38. Zwikker, C.; Kosten, C. W., *Sound absorbing materials*. Elsevier: 1949.

39. Delany, M.; Bazley, E., Acoustical properties of fibrous absorbent materials. *Applied acoustics* **1970,** *3* (2), 105-116.

40. Biot, M. A., Mechanics of deformation and acoustic propagation in

porous media. *Journal of applied physics* **1962,** *33* (4), 1482-1498.

41. Miki, Y., Acoustical properties of porous materials-Modifications of Delany-Bazley models. *Journal of the Acoustical Society of Japan (E)* **1990,** *11* (1), 19-24.

42. Attenborough, K., Acoustical characteristics of rigid fibrous absorbents and granular materials. *The journal of the acoustical society of america* **1983,** *73* (3), 785-799.

43. Perrot, C.; Chevillotte, F.; Panneton, R., Bottom-up approach for microstructure optimization of sound absorbing materials. *The Journal of the Acoustical Society of America* **2008,** *124* (2), 940-948.

44. Perrot, C.; Chevillotte, F.; Panneton, R., Dynamic viscous permeability of an open-cell aluminum foam: Computations versus experiments. *Journal of Applied Physics* **2008,** *103* (2), 024909.

45. Perrot, C.; Chevillotte, F.; Tan Hoang, M.; Bonnet, G.; Bécot, F.-X.; Gautron, L.; Duval, A., Microstructure, transport, and acoustic properties of open-cell foam samples: Experiments and three-dimensional numerical simulations. *Journal of Applied Physics* **2012,** *111* (1), 014911.

46. Zieliński, T. G., Microstructure-based calculations and experimental results for sound absorbing porous layers of randomly packed rigid spherical beads. *Journal of Applied Physics* **2014,** *116* (3), 034905.

47. Brown, R. J., Connection between formation factor for electrical resistivity and fluid-solid coupling factor in Biot's equations for acoustic waves in fluid-filled porous media. *Geophysics* **1980,** *45* (8), 1269-1275.

48. ASTM, E., 1050-12:"Standard test method for impedance and absorption of acoustical materials using tube, two microphones and a digital frequency analysis system", Standard, American Society for Testing and Materials, 2012. *Cited on*, 146.

49. Moreira, E.; Coury, J., The influence of structural parameters on the permeability of ceramic foams. *Brazilian Journal of Chemical Engineering* **2004,** *21* (1), 23-33.

50. Zhu, H.; Knott, J.; Mills, N., Analysis of the elastic properties of open-cell foams with tetrakaidecahedral cells. *Journal of the Mechanics and Physics of Solids* **1997,** *45* (3), 319327-325343.

51. Simone, A.; Gibson, L., Effects of solid distribution on the stiffness and strength of metallic foams. *Acta Materialia* **1998,** *46* (6), 2139-2150.

52. Montminy, M. D.; Tannenbaum, A. R.; Macosko, C. W., The 3D structure of real polymer foams. *Journal of colloid and interface science* **2004,** *280* (1), 202-211.

53. Gong, L.; Kyriakides, S.; Jang, W.-Y., Compressive response of open-cell foams. Part I: Morphology and elastic properties. *International Journal of Solids and Structures* **2005,** *42* (5), 1355-1379.

초 록

본 연구에서는 자동차의 흡·차음재로 사용되는 폴리우레탄 폼의 셀 개폐도가 흡음률에 미치는 영향을 규명하고 최적의 셀 개폐도를 제안하였다. 개폐도가 제어된 폴리우레탄 폼 시편제작을 위해 화학적 기포개방제 PEG 2000 (polyethylene glycol, Mw=2000 g/mol)이 폴리올 레진에 각각 3 또는 6 wt% 첨가하여 시편을 제조하였으며 각각의 흡음률을 측정하였다. 측정결과를 수치해석 값과 비교하기 위하여, 단위 셀 (periodic unit cell)과 흡음 매개변수를 이용하여 미세 셀의 유동해석을 수행함과 동시에 JCA 모델을 통한 거시적 스케일의 흡음률 측정기에 대한 이론적인 분석을 하였다. 두 분석 결과, 기포개방제가 3 wt% 첨가된 폼 샘플과 15% 개폐도 단위 셀의 흡음률 경향이 거의 일치하며 가장 뛰어난 최적의 흡음 성능을 나타내었다. 이는 공기 중의 음파가 폼 내부를 통과할 때 내부통로의 복잡한 정도를 나타내는 흡음 매개변수인 뒤틀림도 (tortuosity)와 개폐도의 연관성이 매우 크기 때문이라고 추론하였다. 본 연구에서 제작된 40 K (=40 kg/m^3) 폼은 현재 산업에서 사용되고 있는 80 K 폼과 비교할 때 밀도는 50%나 절감하였음에도 불구하고 더 우수한 흡음성능을 나타내었다. 따라서, 이러한 저밀도 폴리우레탄 흡음 폼은 향후 자동차의 경량화와 흡음성능을 모두 만족시키며 연비개선에서도 큰 향상을 보여줄 것이라 기대된다.

주요어: 셀 개폐도, 폴리우레탄 폼, 흡음률, PEG 2000, JCA Model, 뒤틀림도
학 번: 2015-22744